JOURNAL OF SOLID STATE CHEMISTRY **122,** 221–230 (1996)
ARTICLE NO. 0105

Crystal Chemistry of $HgBa_2Ca_{n-1}Cu_nO_{2n+2+\delta}$ (n = 1, 2, 3, 4) Superconductors[1]

M. Paranthaman* and B. C. Chakoumakos†

*Chemical and Analytical Sciences Division, Oak Ridge National Laboratory, Oak Ridge, Tennessee 37831-6100; and
†Solid State Division, Oak Ridge National Laboratory, Oak Ridge, Tennessee 37831-6393

Received August 31, 1995; in revised form December 11, 1995; accepted December 13, 1995

Constant wavelength neutron powder diffraction data at room temperature were used to refine the crystal structures of $HgBa_2Ca_{n-1}Cu_nO_{2n+2+\delta}$ (n = 1, 2, 3, 4) superconductors, which were synthesized by solid-state reaction of the component oxides. Samples annealed both in oxygen and argon atmospheres were examined. Rietveld refinements converged to values of R_{wp} = 8–10% and χ^2 = 1.1–1.7 using a tetragonal cell with $P4/mmm$ symmetry. The $HgBa_2CuO_{4+\delta}$, $HgBa_2CaCu_2O_{6+\delta}$, and $HgBa_2Ca_2Cu_3O_{8+\delta}$ (n = 1, 2, and 3) samples were nearly single phase, whereas the $HgBa_2Ca_3Cu_4O_{10+\delta}$ (n = 4) sample was primarily a mixture of the n = 3 and 4 phases. For increasing n, the oxygen-annealed samples exhibit T_c (diamagnetic onsets) of 94, 123, 134, and 124 K, respectively, and a contraction of the CuO_2 sheets (lattice parameter a). The highest T_c sample, $HgBa_2Ca_2Cu_3O_{8+\delta}$, has the shortest apical Cu–O bond. Consistently, the atomic displacement parameter for Hg is large. For refinements in which the Hg atomic displacement parameter is fixed at a more reasonable value, occupancies of the Hg site are significantly less than full for the $n > 1$ samples, suggesting that the Hg site is deficient and/or possibly occupied by atoms with smaller scattering lengths, e.g., Cu. The oxygen site within the Hg layer is partially occupied, and its occupation increases with increasing n. For the argon-annealed samples, the cell volume increases slightly due to the isotropic increase of both the cell parameters and T_c decreases. For $HgBa_2CaCu_2O_{6+\delta}$, the occupancy of the oxygen site within the Hg layer decreases upon annealing in argon, yet the T_c increased, implying that the initial carrier concentration is in the overdoped regime.

I. INTRODUCTION

Following the discoveries of high-temperature superconductivity in the Hg–Ba–Cu–O system by Putilin *et al.* (1), and in the Hg–Ba–Ca–Cu–O system by Schilling *et al.* (2), a family of single-Hg–O layered compounds with the general formula $HgBa_2Ca_{n-1}Cu_nO_{2n+2+\delta}$ (n = 1–8) was identified (3–6). The crystal structures exhibited in the homologous series are shown in Fig. 1. $HgBa_2CuO_{4+\delta}$ (referred to as Hg-1201) is the first member of the series and this is similar to the single-Tl–O layered series $TlBa_2Ca_{n-1}Cu_nO_{2n+3}$. Hg-1201 has the highest T_c (up to 97 K) among the known cuprate superconductors with a single Cu–oxide layer per unit cell (7–10). Hg-1201 has tetragonal crystal symmetry, space group $P4/mmm$, and lattice parameters a = 3.876 Å and c = 9.515 Å (7). The structural arrangement of $HgBa_2CuO_{4+\delta}$ is similar to that of $TlBa_2CuO_{5-\delta}$ except that the former has a rock-salt layer of HgO_δ (with δ very small, ~0.01–0.06; although this δ seems to vary much with different synthetic routes). This depletion is attributed to the preferred dumbbell coordination of the Hg^{2+} ions (11). The latter compound has a rock-salt layer of $TlO_{1-\delta}$ (with a slight oxygen depletion producing either a distorted octahedron or a five-coordinated polyhedron for thallium ions). The n = 2 member, $HgBa_2CaCu_2O_{6+\delta}$ (Hg-1212 also has tetragonal crystal symmetry, space group $P4/mmm$, and lattice parameters a = 3.858 Å and c = 12.656 Å (12). High quality films of Hg-1212 phase with a T_c of 124 K have been grown by pulsed laser deposition (13). The n = 3 member, $HgBa_2Ca_2Cu_3O_{8+\delta}$ (Hg-1223), has the highest T_c of 135 K with the "optimal doping" among all the Hg compounds and as well as other cuprate superconductors presently known (14). Hg-1223 has tetragonal crystal symmetry, space group $P4/mmm$ and lattice parameters a = 3.852 Å and c = 15.83 Å (14). The initial difficulty in synthesizing highly pure phase Hg-1223 samples was overcome by several methods, which include single-step synthesis of simple metal oxides (14), high-pressure synthesis (3), and a controlled vapor–solid reaction technique (15). The onset of superconductivity above 150 K in Hg-1223 samples has been observed at high pressures (16, 17). This implies that the "as-synthesized" Hg-1223 samples are in the underdoped regime. This underdoped

[1] The U.S. Government's right to retain a nonexclusive royalty-free license in and to the copyright covering this paper, for governmental purposes, is acknowledged.

0022-4596/96 $18.00

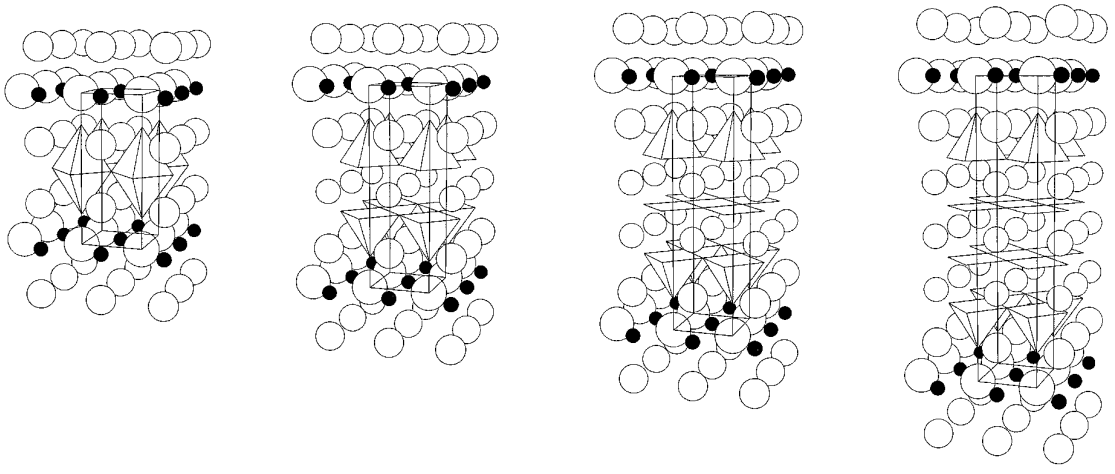

FIG. 1. Orthographic projections of the atomic arrangements of the cuprate superconductor family, left-to-right, $n = 1$, 2, 3, and 4. Oxygen coordinations around the Cu atoms are shown as polyhedra. The large open circles represent Hg, the medium open circles are Ba, and the small open circles are Ca. The solid circles are the partially occupied oxygen sites. Unit cell boxes are outlined.

behavior is confirmed by our thermopower measurements (18). The $n = 4$ member, $HgBa_2Ca_3Cu_4O_{10+\delta}$ (Hg-1234), has a T_c up to 125 K. Hg-1234 has a tetragonal crystal symmetry with space group $P4/mmm$ and lattice parameters $a = 3.858$ Å and $c = 19.011$ Å (3, 4). Through high-pressure methods, mixed phase samples containing as many as eight Cu–oxide layers ($n = 8$) were made by Scott *et al.* (5) with T_c values reaching <90 K for $n \geq 7$.

Neutron powder diffraction results on the crystal structures of various Hg phases, Hg-1201 (19, 20), Hg-1212 (12, 20–24), Hg-1223 (23, 25–27), and Hg-1245 (28), are available in the literature. Unfortunately, some of the neutron data were obtained on multiphase samples. We have successfully made single-phase samples of various Hg phases by single-step synthesis of pure oxides. The exception was Hg-1234 which was primarily a mixture of Hg-1223 and Hg-1234. Also, we have used the neutron powder data analysis as a tool to check the purity of our Hg samples. This report contains detailed neutron powder diffraction data analysis of both oxygen- and argon-annealed samples of $HgBa_2CuO_{4+\delta}$, $HgBa_2CaCu_2O_{6+\delta}$, $HgBa_2Ca_2Cu_3O_{8+\delta}$, and $HgBa_2Ca_3Cu_4O_{10+\delta}$ at room temperature. The neutron powder diffraction data for $HgBa_2Ca_3Cu_4O_{10+\delta}$ (Hg-1234) is reported here for the first time.

II. EXPERIMENTAL

The bulk samples of $HgBa_2Ca_{n-1}Cu_nO_{2n+2+\delta}$ ($n = 1$, 2, 3, and 4) were prepared by a solid-state reaction from stoichiometric mixtures of individual metal oxides. High purity 99.998% HgO and 99.999% CuO were used. Highly pure BaO was obtained by heating 99.997% pure $BaCO_3$ in a high vacuum at 1000°C for several days. The CaO was obtained from 99.97% pure $CaCO_3$ by heating in air at 1000°C for ~4 h. The starting mixtures were ground well and pressed into a pellet. All the chemical handling was done in a dry box. The pellet (typically 3.2 mm diameter, 10 mm length, and ~900 mg mass) was placed in an alumina sheath (to avoid samples reacting with the quartz tubes) and then the alumina tube (3.3 mm i.d. × 5.2 mm o.d. × 40 mm length) was introduced into a quartz tube, which was evacuated and sealed. Exposure to the ambient atmosphere was minimized (to avoid contamination with H_2O and CO_2 present in the atmosphere) while tranferring the pellet into the quartz tube. The sealed quartz capsule (typically 6 mm i.d. × 11 mm o.d. × 75 mm length) was placed in a long horizontal steel tube which was kept inside a furnace. The samples were heated slowly in 8–10 h to 800°C for $HgBa_2CuO_{4+\delta}$, 820°C for $HgBa_2CaCu_2O_{6+\delta}$, and 860°C for both $HgBa_2Ca_2Cu_3O_{8+\delta}$ and $HgBa_2Ca_3Cu_4O_{10+\delta}$; held at that temperature for 6 h; and then slowly cooled to room temperature in 8 h. The quartz tube remained intact and a drop of mercury was found sometimes in the tube. For neutron work, two batches of samples were made at the same time using identical conditions. All the samples were post-annealed in oxygen at 300°C for 6 h and slow cooled to room temperature in oxygen. Some of the oxygen-annealed samples were reannealed in argon at 300°C for 6 h and slowly cooled to room temperature in argon.

Measurements of the ac susceptibility were conducted on bulk samples in nominally zero dc field using a Lakeshore Model 7025 susceptometer. These experiments were conducted using a 125 Hz ac field with amplitude of 1 G. Superconducting transition temperatures were obtained as the diamagnetic onset temperature upon warming from low temperature. The structure of the material was established via X-ray diffraction (XRD). XRD samples were prepared by powdering a chip from the bulk, dispersing it

in toluene, and depositing a thin portion on a single-crystal Si substrate. A Philips Model XRG3100 diffractometer with Cu$K\alpha$ radiation was used to perform the experiment. Neutron diffraction data were collected using the HB4 powder diffractometer at the High-Flux Isotope Reactor at ORNL. A Ge (115) monochromator with $2\theta_M = 80°$ was employed. This monochromator selects an incident neutron beam of $\lambda \approx 1.4$ Å. The wavelength was determined more precisely to be 1.4177(1) Å on the basis of unit cell refinements for nickel and silicon standards. Soller slit collimators of 12′ and 20′ are positioned before and after the monochromator crystal, respectively. An array of 32 equally spaced (2.7°) ^{3}He detectors (2.54 cm diameter, 0.413 MPa pressure), each with a 6′ mylar foil Soller collimator, can be step-scanned over a range of up to 40° for scattering angles between 11° and 135°. The samples were wrapped in Al foil (3 mm o.d. × 6 cm) for data collection at 295 K over the 2θ range from 11° to 135° in steps of 0.05°, counting for −250 s/step. For these data collections, the detector array was scanned in two segments, from 11° and from 40.2° 2θ, each for 10.8°. These scan parameters have the effect of overlapping up to 8 detectors for steps in the middle of the pattern, which serves to average the counting efficiency for each detector. We used 1.5 g samples which gave peak-to-background count ratios in the range 9–5.

The least-squares structural refinements were made by the Rietveld method (29) using the GSAS software (30). The pseudo-Voigt peak-profile function as described by Thompson *et al.* (31) was used. The pseudo-Voigt function was integrated using a multiterm Simpson's rule (32). The 2θ difference, ΔT, was modified for asymmetry, A_s, as $\Delta T' = \Delta T + f_i A_s/\tan 2\theta$. The width of the peak, σ^2, was allowed to vary with 2θ as $\sigma^2 = U \tan^2\theta + V \tan\theta + W$, where U, V, and W are the coefficients described by Caglioti *et al.* (33). The values of V and W are fixed as determined for the standard reference material silicon (NIST 640b). The peak-profiles were truncated at 0.3% of the peak height. The background was defined by a cosine Fourier series with three to four terms refined simultaneously with a zero-point correction and as well as the other structural parameters. The coherent scattering lengths used were 12.66 (Hg), 5.25 (Ba), 4.90 (Ca), 7.72 (Cu), 5.81 (O), and 3.45 (Al) fm (34). Intensities were corrected for the Lorentz effect. No absorption correction was applied because μ_R was less than 0.1 for the samples. The data sets were limited to the 2θ angular range of 20° (15° for $n = 1$) to 132°—or to d spacings of 4.082 (5.430 for $n = 1$) to 0.7759 Å. Several weak peaks associated with an unidentified impurity, common to only the Ca-containing samples, were excluded. Weak peaks from the Al foil could also be detected in the raw data, so Al was included in the refinements with a variable cell edge and volume fraction. For the $n = 1$ sample, the Al peaks were excluded. The function minimized in the least-squares procedure was $\Sigma w_i(Y_{i0} - Y_{ic})^2$, where Y_{i0} and Y_{ic} are the observed and calculated intensities at each step i in the pattern. The weight w_i assigned to each step intensity is the reciprocal of the variance σ_i^2 at the ith step and was evaluated by $w_i = 1/\sigma_i^2 \approx n/Y_{i0}$ where n is the number of detectors contributing to the average step intensity. The following agreement factors were calculated:

$$R_p = \Sigma\,|Y_{i0} - Y_{ic}|\,/\Sigma Y_{i0}$$

$$R_{wp} = [\Sigma\, w_i(Y_{i0} - Y_{ic})^2/\Sigma w_i Y_{i0}^2]^{1/2}$$

$$\text{Goodness-of-fit} = \Sigma w_i(Y_{i0} - Y_{ic})^2/(N - P).$$

N and P are the number of observations and adjustable parameters, respectively.

Starting values for the structural parameters for the refinements were obtained from the $TlBa_2Ca_{n-1}Cu_nO_{2n+3}$ data tabulated by Torardi (35), and starting values for the peak-profile function parameters were assigned and held fixed based on previous refinements of standards (36). The least-squares refinements were continued until the sum of the squared errors, i.e., (parameters shifts/e.s.d.)^2, was less than 1%. In the final refinements, atomic displacement parameters for both the Hg site and the partially occupied oxygen site were fixed at more reasonable values. Examples of the observed, calculated, and difference neutron powder diffraction profiles are given in Fig. 2.

III. RESULTS

Rietveld refinements converged to values of R_{wp} = 8–10% and χ^2 = 1.1–1.7 using a tetragonal cell with $P4/mmm$ symmetry. The structural data and agreement indices for each of the refinements are given in Table 1. The quality of the refinements is somewhat limited by the relatively small amounts of sample used which resulted in poor peak-to-background intensity ratios, but this was necessary to minimize the absorption caused by the use of the natural isotropic composition of Hg. Better data would result for samples made with a Hg isotropic composition depleted in Hg-199. Despite this shortcoming, the quality of these refinements to allow a number of observations to be made.

The $n = 1$, 2, and 3 samples are nearly single phase, whereas the $n = 4$ sample is primarily a mixture of the 50 vol% $n = 3$ relative to 50 vol% $n = 4$ phases. For increasing n, the oxygen-annealed samples exhibit, respectivley, T_c onsets of 94, 122, 134, and 125 K and a contraction of the CuO_2 sheets (as shown in Fig. 3). Selected interatomic distances are compared for the oxygen- and argon-annealed samples in Table 2. The apical Cu–O bond is shortest for the sample Hg-1223, exhibiting the highest T_c. Consistently, the atomic displacement parameter for Hg is

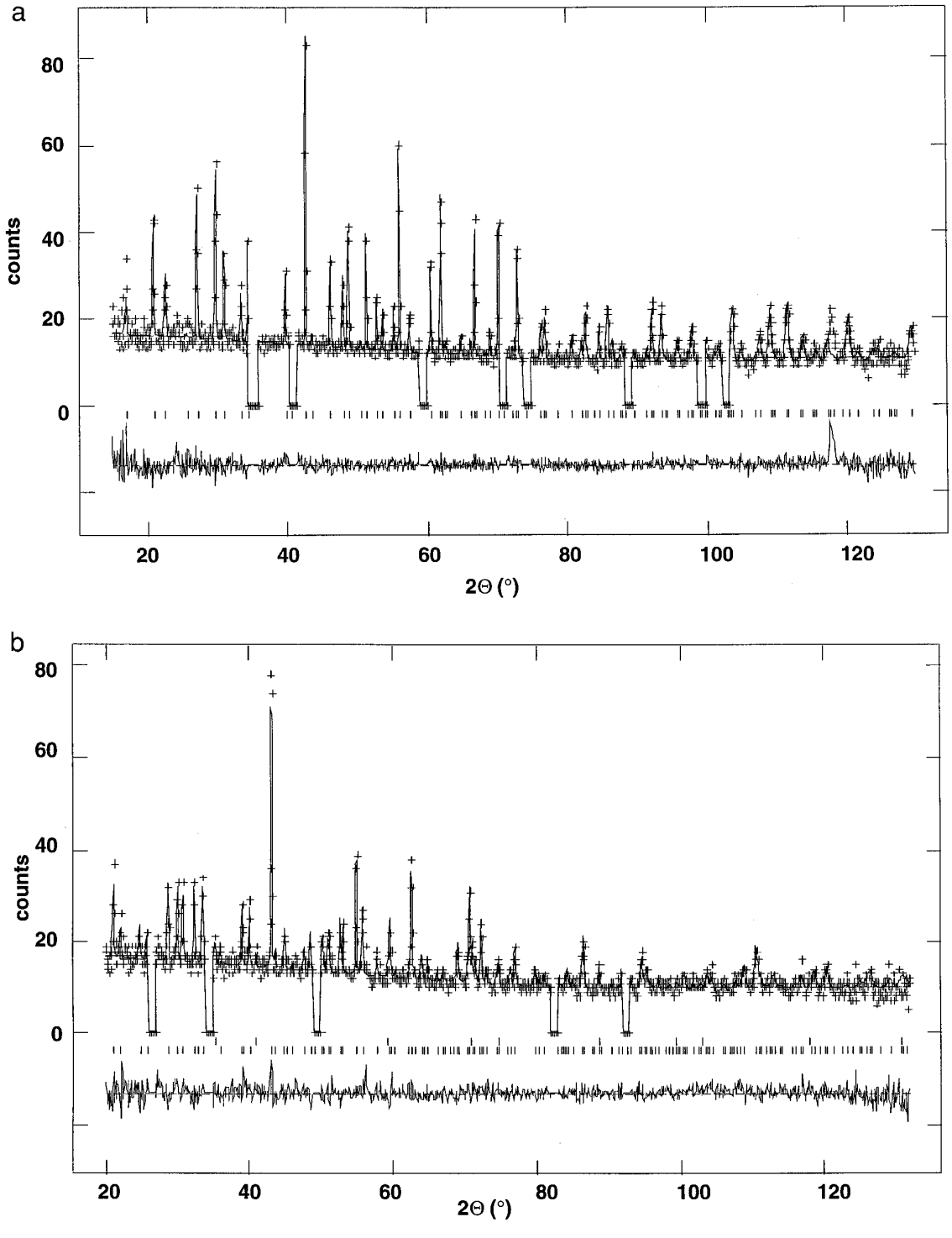

FIG. 2. Observed, calculated, and difference neutron powder diffraction ($\lambda = 1.4177$ Å) profiles for oxygen annealed samples of (a) $HgBa_2CuO_{4+\delta}$, (b) $HgBa_2CaCu_2O_{6+\delta}$, (c) $HgBa_2Ca_2Cu_3O_{8+\delta}$, and (d) $HgBa_2Ca_3Cu_4O_{10+\delta}$. Crosses show the observed intensity points. The vertical bars below the diffraction pattern mark the positions of the allowed reflections, with the majority phase being the lowest set of markers. Reflections from the aluminum sample can were excluded in (a), and included in the refinement for (b), (c), and (d). Additionally, impurity peaks common to all of the Ca-containing samples were excluded. The nominal composition $HgBa_2Ca_3Cu_4O_{10+\delta}$ produced a mixture of the intended phase plus $HgBa_2Ca_2Cu_3O_{8+\delta}$.

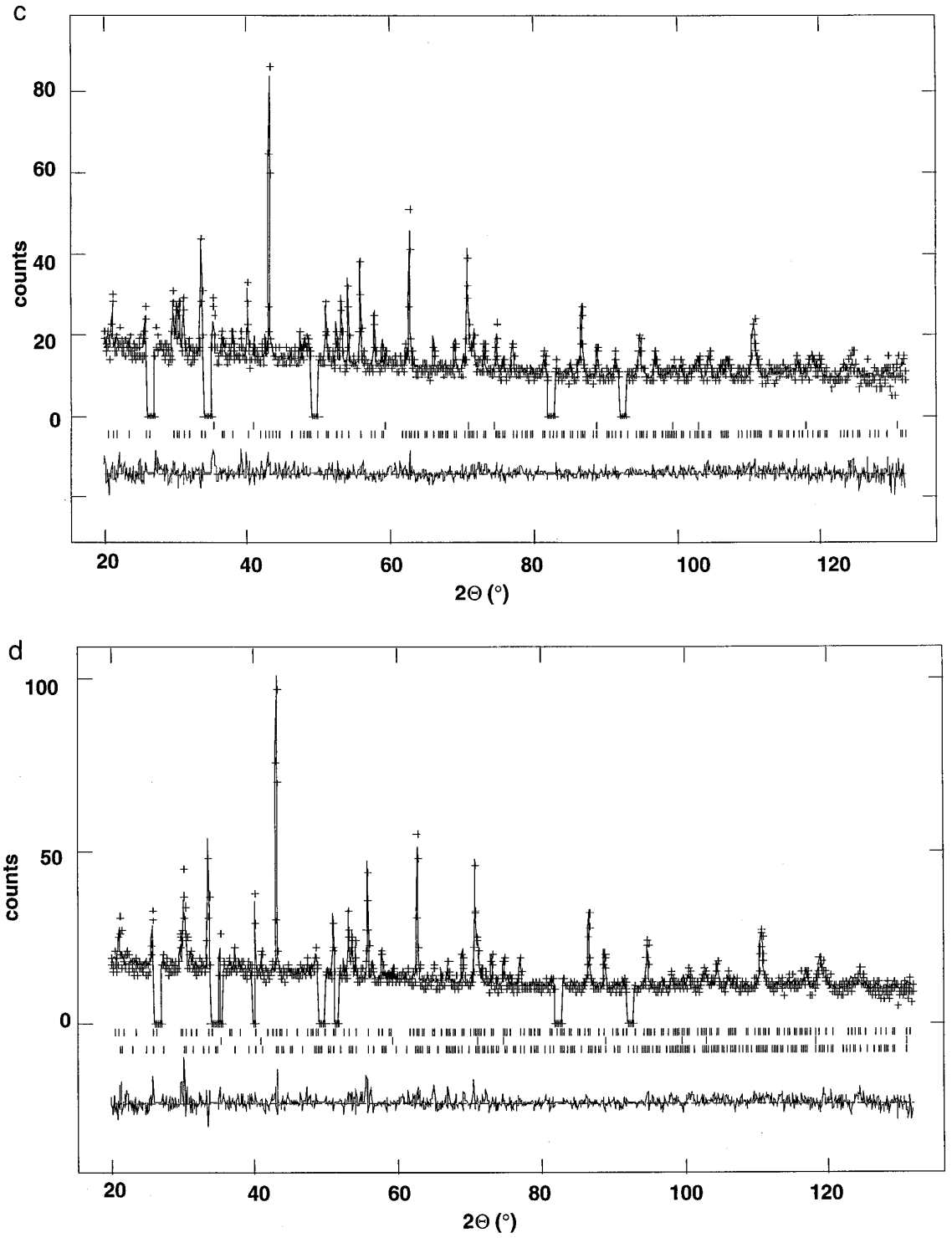

FIG. 2—*Continued*

TABLE 1
Positional[a] and Isotropic Displacement Parameters (Å^2)[b] for $HgBa_2Ca_{n-1}Cu_nO_{2n+2+\delta}$ (n = 1, 2, 3, 4)

	$HgBa_2CuO_{4+\delta}$ annealed in	$HgBa_2CaCu_2O_{6+\delta}$ annealed in		$HgBa_2Ca_2Cu_3O_{8+\delta}$ annealed in		$HgBa_2Ca_3Cu_4O_{10+\delta}$[c] annealed in	
	Oxygen	Oxygen	Argon	Oxygen	Argon	Oxygen	Argon
Hg site	1*a*	1*a*	1*a*	1*a*	1*a*	1*a*	1*a*
x	0.0	0.0	0.0	0.0	0.0	0.0	0.0
y	0.0	0.0	0.0	0.0	0.0	0.0	0.0
z	0.0	0.0	0.0	0.0	0.0	0.0	0.0
U	0.008[d]	0.008[d]	0.008[d]	0.008[d]	0.008[d]	0.008[d]	0.008[d]
n	0.99 (1)	0.87 (1)	0.90 (1)	0.83 (1)	0.87 (2)	0.84 (5)	0.82 (5)
Ba site	2*h*	2*h*	2*h*	2*h*	2*h*	2*h*	2*h*
x	0.5	0.5	0.5	0.5	0.5	0.5	0.5
y	0.5	0.5	0.5	0.5	0.5	0.5	0.5
z	0.3005 (5)	0.2202 (7)	0.2216 (6)	0.1749 (6)	0.1740 (7)	0.142 (1)	0.138 (1)
U	0.007 (1)	0.014 (2)	0.009 (1)	0.006 (2)	0.010 (2)	0.024 (7)	0.021 (6)
Cu(1) site	1*b*	2*g*	2*g*	1*b*	1*b*	2*g*	2*g*
x	0.0	0.0	0.0	0.0	0.0	0.0	0.0
y	0.0	0.0	0.0	0.0	0.0	0.0	0.0
z	0.5	0.3771 (5)	0.3777 (4)	0.5	0.5	0.2502 (8)	0.2509 (8)
U	0.0054 (9)	0.009 (1)	0.006 (1)	0.011 (2)	0.010 (2)	0.0 (3)	0.004 (3)
Cu(2) site	—	—	—	2*g*	2*g*	2*g*	2*g*
x	—	—	—	0.0	0.0	0.0	0.0
y	—	—	—	0.0	0.0	0.0	0.0
z	—	—	—	0.3000 (4)	0.2993 (5)	0.416 (1)	0.417 (1)
U	—	—	—	0.006 (1)	0.008 (1)	0.0 (7)	0.013 (4)
Ca(1) site	—	1*d*	1*d*	2*h*	2*h*	1*d*	1*d*
x	—	0.5	0.5	0.5	0.5	0.5	0.5
y	—	0.5	0.5	0.5	0.5	0.5	0.5
z	—	0.5	0.5	0.3980 (8)	0.3979 (9)	0.5	0.5
U	—	0.005 (2)	0.003 (2)	0.007 (2)	0.003 (2)	0.003 (8)	0.01(1)
Ca(2) site	—	—	—	—	—	2*h*	2*h*
x	—	—	—	—	—	0.5	0.5
y	—	—	—	—	—	0.5	0.5
z	—	—	—	—	—	0.324 (1)	0.324 (1)
U	—	—	—	—	—	0.021 (1)	0.008 (5)

large. The oxygen site within the Hg layer is partially occupied. When possible, unconstrained refinements of the Hg-site occupancy showed no deficiency at this site; however, when the Hg atomic displacement parameter is fixed, the refined occupancy is less than one for the $n > 1$ samples. For the argon-annealed samples the cell volume increases slightly due to the isotropic increase of the cell parameters and T_c decreases. For the $n = 2$ sample the occupancy of the oxygen site within the Hg layer decreases upon annealing in argon; however, the same expected change for the $n = 3$ and 4 samples is not evident due to the poorer precision for these structural parameters. The increase in T_c for the $n = 2$ sample (Table 3) upon Ar annealing implies that the oxygen-annealed sample was somewhat overdoped with respect to holes. The T_c values for the $n = 3$ and 4 samples both decreased upon Ar annealing (Table 3), despite the lack of a measurable change in the oxygen content for these samples, and their initial oxygen-annealed condition is probably near the optimal hole content.

IV. DISCUSSION

An impurity phase is present in the Ca-containing phases, which could not be identified by comparison with other known phases. This also includes the exclusion of the $Ba_2Cu_3O_{5+\delta}$ phase, identified as the main impurity in other preparations of $HgBa_2Ca_2Cu_3O_{8+\delta}$ (27). We acknowledge that the exclusion of impurity peaks can introduce systematic errors in the determination of the structural parameters; however, our refinement results appear to be reasonable as compared with other studies, such as for

TABLE 1—*Continued*

	$HgBa_2CuO_{4+\delta}$ annealed in	$HgBa_2CaCu_2O_{6+\delta}$ annealed in		$HgBa_2Ca_2Cu_3O_{8+\delta}$ annealed in		$HgBa_2Ca_3Cu_4O_{10+\delta}$[c] annealed in	
	Oxygen	Oxygen	Argon	Oxygen	Argon	Oxygen	Argon
O(1) site	2*e*	4*i*	4*i*	2*e*	2*e*	4*i*	4*i*
x	0.0	0.0	0.0	0.0	0.0	0.0	0.0
y	0.5	0.5	0.5	0.5	0.5	0.5	0.5
z	0.0	0.3772 (5)	0.3767 (4)	0.5	0.5	0.248 (1)	0.247 (1)
U	0.008 (1)	0.013 (1)	0.009 (1)	0.014 (2)	0.003 (2)	0.02 (5)	0.020 (4)
O(2) site	2*g*	2*g*	2*g*	4*i*	4*i*	4*i*	4*i*
x	0.0	0.0	0.0	0.0	0.0	0.0	0.0
y	0.0	0.0	0.0	0.5	0.5	0.5	0.5
z	0.2054 (5)	0.1556 (6)	0.1554 (5)	0.3023 (5)	0.3020 (6)	0.4174 (7)	0.4159 (8)
U	0.013 (1)	0.021 (2)	0.019 (2)	0.005 (1)	0.009 (1)	0.0 (3)	0.011 (4)
O(3) site	1*c*	1*c*	1*c*	2*g*	2*g*	2*g*	2*g*
x	0.5	0.5	0.5	0.0	0.0	0.0	0.0
y	0.5	0.5	0.5	0.0	0.0	0.0	0.0
z	0.0	0.0	0.0	0.1260 (6)	0.1243 (6)	0.102 (1)	0.104 (1)
U	0.01[d]	0.01[d]	0.01[d]	0.015 (2)	0.010 (2)	0.015 (6)	0.034 (5)
n	0.1 (1)	0.32 (3)	0.21 (3)	1.0	1.0	1.0	1.0
O(4) *x*	—	—	—	0.5	0.5	0.5	0.5
y	—	—	—	0.5	0.5	0.5	0.5
z	—	—	—	0.0	0.0	0.0	0.0
U	—	—	—	0.01[d]	0.01[d]	0.01[d]	0.01[d]
n	—	—	—	0.24 (3)	0.28 (4)	0.4 (1)	0.47 (9)
a(Å)	3.8888 (1)	3.8586 (2)	3.8623 (2)	3.8553 (2)	3.8565 (2)	3.8495 (2)	3.8529 (3)
c(Å)	9.5464 (6)	12.697 (1)	12.7104 (8)	15.858 (1)	15.862 (1)	19.003 (1)	18.996 (2)
R_p	7.32	7.80	7.39	7.67	8.45	8.30	8.13
R_{wp}	8.64	9.31	8.81	9.22	10.07	10.16	9.86
χ^2	1.14	1.29	1.47	1.32	1.56	1.64	1.54

[a] Space group *P*4/*mmm*.
[b] The temperature factor in the expression for the structure factor is defined by $\exp[-8\pi^2 U_{iso} \sin^2 \Theta/\lambda^2]$.
[c] 50 vol% $HgBa_2Ca_3Cu_4O_{10+\delta}$:50 vol% $HgBa_2Ca_2Cu_3O_{8+\delta}$ as determined from Rietveld analysis.
[d] Fixed values.

$HgBa_2Ca_2Cu_3O_{8+\delta}$ (27), where several minor impurity phases have been included in the refinements.

Careful study of T_c as a function of the oxygen content for each of the end members should reveal the familiar parabolic T_c dependence, where the oxygen content is indirectly proportional to the hole content. Some evidence for this picture is already available in the literature in preliminary compilations of T_c vs δ. Given that several routes to synthesizing these compounds are in existence and that the post-annealing conditions are also variable, one must be cautious in accepting what are the optimally doped properties.

Various explanations have been proposed to account for the large atomic displacement parameters consistently determined for Hg in these compounds. The atomic displacement parameter, as a regressor variable in the refinement model, describes the time- and space-averaged displacements of the atom from its mean position. Here the vibrational motion could be ascribed to thermal motion, to positional disorder generated by the partially occupied oxygen site, to incomplete occupation of the Hg site, and/or to partial substitution of another element at the Hg site. Site occupancy refinements in this study indicate that the Hg site is fully occupied when the atomic displacement parameter is also varied. A survey of other well-ordered structures containing Hg in dumbbell coordination with oxygen, e.g., $SrHgO_2$ (37), M_2HgO_2 with M = Li, Na, K, Rb, and Cs (38), trigonal HgO (39), orthorhombic HgO, and $2HgO \cdot NaI$ (40), suggests that the large temperature factors for the Hg atoms occur only when the symmetry constrains the O–Hg–O bond angle to be 180°. For compounds, such as orthorhombc HgO and trigonal HgO, in which the dumbbell coordination of Hg is unconstrained by symmetry, the O–Hg–O angles are less than 180°, e.g., 178° and 175°, respectively. The $2HgO \cdot HaI$ structure, which contans infinite zigzag chains like those in ortho-

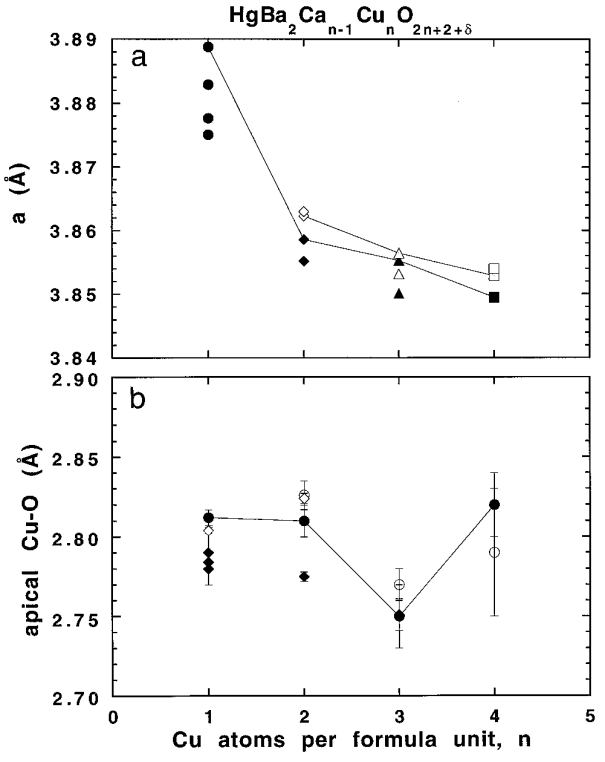

FIG. 3. The *a* cell edge (Å) (a) and the apical Cu–O bond length (b) for different values of *n*, the number of Cu atoms per $HgBa_2Ca_{n-1}Cu_nO2_{n+2+\delta}$ formula unit. The open symbols show oxygen-deficient samples and the solid symbols show oxygen-rich (annealed) samples. The lines connect data determined from this study. The other data shown are taken from the literature.

rhombic HgO embedded in a mixture of Na^+ and I^- ions, is an exception. It has an unconstrained O–Hg–O bond angle that is sterically constrained to be linear by three neighboring I atoms. The dumbbell coordination of Hg in the M_2HgO_2 structure-type is also constrained by symmetry to be linear, although no thermal parameters have been reported for any members of this family of compounds. Given that a bent O–Hg–O angle might be more energetically favored, a large thermal parameter would be expected for a Hg atom in dumbbell coordination constrained to be 180°. This notion is contrary to expectations based on simple electrostatic or orbital hybridization arguments, which predict a linear molecular arrangement for a two-coordinated d^{10} ion. An alterantive picture emerges if the Hg atomic displacement parameters are fixed at smaller, more reasonable values. In these cases, the refined occupation of the Hg site is significantly less than one for the $n > 1$ samples. This suggests that the Hg site is deficient and/or also occupied by atoms with smaller scattering lengths, e.g., Cu. This explanation is appealing, since isostructural $CuBa_2Ca_3Cu_4O_{12}$ compounds with a T_c of 116 K can be synthesized at high pressure (41).

That the Hg cuprate family is similar structurally to other polysomatic series of cuprate superconductors is evident in Fig. 4, where the layer-stacking repeat for the primitive cell minus that of the respective $n = 1$ member is plotted versus the mol% $CaCuO_2$ for five series. The thickness of the infinite-layer-type $CaCuO_2$ closely matches the $CaCuO_2$ layer module thickness derived from these polysomatic series, and the $n > 1$ members simply contain additions of exact multiples of this layer module. This perspective suggests that the thickness of the charge reservoir blocks is a key feature which correlates with the intrinsic behavior of the magnetic irreversibility field among the different series (42). Although the magnetic irreversibility field behavior tends to be dominantly controlled by the microstructure of the material, for materials with similar microstructures, the smaller the spacing of the reservoir blocks, the weaker the temperature dependence of the irreversibility field. For example, comparing the same *n*-member, the intrinsic irreversibility field should improve in the series two-layer BiO cuprate < two-layer TlO cuprate < one-layer TlO cuprate < Hg cuprate < TlPb cuprate.

V. CONCLUSIONS

Our investigations on the $HgBa_2Ca_{n-1}Cu^nO_{2n+2+\delta}$ (n = 1–4) system has led to the following conclusions.

1. High quality samples of $HgBa_2CuO_{4+\delta}$, $HgBa_2CaCu_2O_{6+\delta}$, $HgBa_2Ca_2Cu_3O_{8+\delta}$, and $HgBa_2Ca_3Cu_4O_{10+\delta}$ have been synthesized by solid-state reaction from simple metal oxide components.

2. The $HgBa_2CuO_{4+\delta}$, $HgBa_2CaCu_2O_{6+\delta}$, and $HgBa_2Ca_2Cu_3O_{8+\delta}$ are nearly single-phase as determined by Rietveld analysis of neutron powder diffraction data. The $HgBa_2Ca_3Cu_4O_{10+\delta}$ sample was primarily a mixture of the $n = 3$ and 4 phases.

3. Rietveld refinements of all the phases converged to values of R_{wp} = 8–10% and χ^2 = 1.1–1.7 using a tetragonal unit cell with $P4/mmm$ symmetry.

4. All the as-synthesized samples were annealed in oxygen, and most of them were reannealed in argon. The T_c values, onset of diamagnetism, of the oxygen-annealed samples are 94, 122, 134, and 125 K for the n = 1, 2, 3, and 4 samples, respectively. For the argon-annealed samples the T_c values are 126, 124, and 120 K for the n = 2, 3, and 4 samples, respectively.

5. The oxygen site within the Hg layer is partially occupied, and as *n* increases this occupation increases and the *a* lattice parameter (i.e., CuO_2 sheets) contracts.

6. The highest T_c sample, $HgBa_2Ca_2Cu_3O_{8+\delta}$, has the shortest apical Cu–O bond.

7. The atomic displacement parameter for Hg is consistently large and the occupancies of the Hg site are significantly less than full for the $n > 1$ samples.

TABLE 2
Selected Interatomic Distances for $HgBa_2Ca_{n-1}Cu_nO_{2n+2+\delta}$ (n = 1, 2, 3, 4)

	$HgBa_2CuO_{4+\delta}$ annealed in	$HgBa_2CaCu_2O_{6+\delta}$ annealed in		$HgBa_2Ca_2Cu_3O_{8+\delta}$ annealed in		$HgBa_2Ca_3Cu_4O_{10+\delta}$ annealed in	
	Oxygen	Oxygen	Argon	Oxygen	Argon	Oxygen	Argon
Hg–O(2) × 2	1.961 (5)	1.976 (8)	1.976 (7)	—	—	—	—
Hg–O(3) × 4	2.7498 (1)	2.7284 (1)	2.7311 (1)	—	—	—	—
Hg–O(3) × 2	—	—	—	2.00 (1)	1.97 (1)	1.94 (2)	1.97 (3)
Hg–O(4) × 4	—	—	—	2.7243 (1)	2.7270 (1)	2.7220 (1)	2.7244 (2)
Ba–O(1) × 4	2.721 (3)	2.774 (7)	2.759 (6)	—	—	2.77 (2)	2.83 (2)
Ba–O(2) × 4	2.895 (2)	2.849 (4)	2.858 (3)	2.79 (1)	2.80 (2)	—	—
Ba–O(3) × 1	2.869 (5)	2.79 (1)	2.818 (8)	—	—	—	—
Ba–O(3) × 4	—	—	—	2.834 (4)	2.839	2.83 910	2.80 (1)
Ba–O(4) × 1	—	—	—	2.77 (1)	2.76 (1)	2.72 (2)	2.62 (2)
Cu(1)–O(1) × 4	1.9444 (1)	1.9293 (1)	1.9312 (1)	1.9280 (2)	1.9282 (1)	1.9252 (6)	1.9273 (8)
Cu(1)–O(2) × 2	2.812 (5)	—	—	—	—	—	—
Cu(1)–O(2) × 1	—	2.81 (1)	2.826 (9)	2.75 (1)	2.77 (1)	—	—
Cu(1)–O(3) × 1	—	—	—	—	—	2.82 (2)	2.79 (4)
Cu(2)–O(2) × 4	—	—	—	—	—	1.9249 (2)	1.9267 (5)
Ca(1)–O(1) × 8	—	2.481 (4)	2.487 (4)	—	—	—	—
Ca(1)–O(1) × 4	—	—	—	2.516 (9)	2.518 (9)	—	—
Ca(1)–O(2) × 4	—	—	—	2.453 (8)	2.456 (9)	—	—
Ca(1)–O(2) × 8	—	—	—	—	—	2.48 (1)	2.50 (1)
Ca(2)–O(1) × 4	—	—	—	—	—	2.40 (2)	2.40 (1)
Ca(2)–O(2) × 4	—	—	—	—	—	2.61 (2)	2.60 (2)

8. For the n = 2 and 3 members, the argon-annealed samples have a slightly increased cell volume as compared with the oxygen-annealed samples. This is due to the isotropic increase of both the cell parameters.

9. For $HgBa_2CaCu_2O_{6+\delta}$, the occupancy of the oxygen site within the Hg layer decreases upon annealing in argon, yet the T_c increased, implying that the initial carrier concentration is in the overdoped regime.

10. The Hg cuprate family is structurally similar to other

TABLE 3
Superconducting Transition Temperatures[a] (K) for $HgBa_2Ca_{n-1}Cu_nO_{2n+2+\delta}$ (n = 1, 2, 3, 4)

Sample	Phase	Annealed in: Oxygen	Annealed in: Argon
PAR218	$HgBa_2CuO_{4+\delta}$	94	—
PAR219	$HgBa_2Cu_2O_{6+\delta}$	122	126
PAR221	$HgBa_2Ca_2Cu_3O_{8+\delta}$	134	124
PAR222[b]	$HgBa_2Ca_3Cu_4O_{10+\delta}$	125	120
	$HgBa_2Ca_2Cu_3O_{8+\delta}$	134	127

[a] As determined by the onset of diamagnetism.

[b] 50 vol% $HgBa_2Ca_3Cu_4O_{10+\delta}$; 50 vol% $HgBa_2Ca_2Cu_3O_{8+\delta}$ as determined from Rietveld analysis.

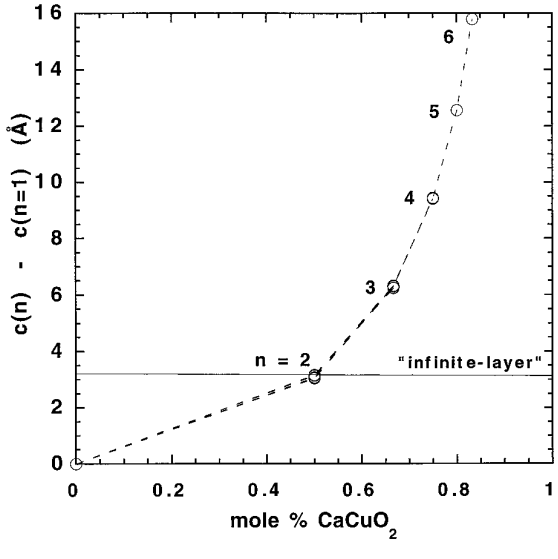

FIG. 4. The difference of the c-lattice constant and c for the n = 1 member for five polysomatic series of cuprate superconductors, derived by insertion of $CaCuO_2$ layer modules. Data for $Bi_2Sr_2Ca_{n-1}Cu_nO_{2n+4}$ (n = 1–3); $Tl_2Ba_2Ca_{n-1}Cu_nO_{2n+4}$ (n = 1–4); $TlBa_2Ca_{n-1}Cu_nO_{2n+3}$($n$ = 1–4); $HgBa_2Ca_{n-1}Cu_nO_{2n+2+\delta}$ (n = 1–6); (Tl, Pb)$Sr_2Ca_{n-1}Cu_nO_{2n+3}$ (n = 1–3). In all cases, the c parameters are for the primitive cell choices. The infinite-layer-type $CaCuO_2$ is plotted as a line to show that its thickness closely matches the $CaCuO_2$ layer module thickness.

polysomatic series of cuprate superconductors. The thickness of the infinite-layer-type $CaCuO_2$ closely matches the $CaCuO_2$ layer module (superconducting blocks) thickness derived from all the known polysomatic series (see Fig. 4), and the $n > 1$ members simply contain additions of exact multiples of this layer module.

ACKNOWLEDGMENTS

Thanks are due to Patrick Martin for technical assistance with the a.c. susceptibility measurements. This research was sponsored by the Division of Materials Sciences, Office of Basis Energy Sciences, U.S. Department of Energy and technology development was funded by the U.S. Department of Energy Office of Advanced Utility Concepts-Superconducting Technology Program, both under Contract DE-AC05-84OR21400 with Lockheed-Martin Energy Systems.

REFERENCES

1. S. N. Putilin, E. V. Antipov, O. Chmaissem, and M. Marezio, *Nature* **362,** 226 (1993).
2. A. Schilling, M. Cantoni, J. D. Guo, and H. R. Ott, *Nature* **363,** 56 (1993).
3. E. V. Antipov, S. M. Loureiro, C. Chaillout, J. J. Capponi, P. Bordet, J. L. Tholence, S. N. Putilin, and M. Marezio, *Physica C* **215,** 1 (1993).
4. M. Paranthaman, in preparation.
5. B. A. Scott, E. Y. Suard, C. C. Tsuei, D. B. Mitzi, T. R. McGuire, B.-H. Chen, and D. Walker, *Physica C* **230,** 239 (1994).
6. S. M. Loureiro, E. V. Antipov, E. T. Alexandre, E. Kopnin, M. F. Gorius, B. Souletie, M. Perroux, R. Argoud, O. Gheorghe, J. L. Tholence, and J. J. Capponi, *Physica C* **325–240,** 905 (1994).
7. M. Paranthaman, J. R. Thompson, Y. R. Sun, and J. Brynestad, *Physica C* **213,** 271 (1993).
8. C. K. Subramaniam, M. Paranthaman, and A. B. Kaiser, *Physica C* **222,** 47 (1994).
9. M. Paranthaman, J. R. Thompson, Y. R. Sun, J. Brynestad, and D. M. Kroeger, *Appl. Supercond.* **2,** 359 (1994).
10. Y. Y. Xue, Q. Xiong, F. Chen. Y. Cao, L. M. Liu, A. J. Jacobson, and C. W. Chu, *Physica C* **235–240,** 901 (1994) and references therein.
11. J. L. Wagner, P. G. Radaelli, D. G. Hinks, J. D. Jorgensen, J. F. Mitchell, B. Dabrowski, G. S. Knapp, and M. A Beno, *Physica C* **210,** 447 (1993).
12. R. G. Radaelli, J. L. Wagner, B. A. Hunt, M. A. Hunt, M. A. Beno, G. S. Knapp, J. D. Jorgensen, and D. G. Hinks, *Physica C* **216,** 29 (1993).
13. C. C. Tsuei, A. Gupta, G. Trafas, and D. Mitzi, *Science* **263,** 1259 (1994).
14. M. Paranthaman, *Physica C* **222,** 7 (1994).
15. R. L. Meng, L. Beauvais, X. N. Zhang, Z. J. Huang, Y. Y. Sun, Y. Y. Xue, and C. W. Chu, *Physica C* **216,** 21 (1993).
16. C. W. Chu, L. Gao, F. Chen, Z. J. Huang, R. L. Meng, and Y. Y. Xue, *Nature* **365,** 323 (1993).
17. M. Nunez-Regueiro, J.-L. Tholence, E. V. Antipov, J.-J. Capponi, and M. Marezio, *Science* **262,** 97 (1993).
18. C. K. Subramaniam, M. Paranthaman, and A. B. Kaiser, *Phys. Rev. B* **51,** 1330 (1995).
19. O. Chmaissem, Q. Huang, S. N. Putilin, M. Marezio, and A. Santoro, *Physica C* **212,** 259 (1993).
20. B. A. Hunter, J. D. Jorgensen, J. L. Wagner, P. G. Radaelli, D. G. Hinks, H. Shaked, and R. L. Hitterman, *Physica C* **221,** 1 (1994).
21. E. V. Antipov, J. J. Capponi, C. Chaillout, O. Chmaissem, S. M. Loureiro, M. Marezio, S. N. Putilin, A. Santoro, and J. L. Tholence, *Physica C* **218,** 348 (1993).
22. Q. Huang, J. W. Lynn, R. L. Meng, and C. W. Chu, *Physica C* **218,** 356 (1993).
23. L. M. Finger, R. M. Hazen, R. T. Downs, R. L. Meng, and C. W. Chu, *Physica C* **226,** 216 (1994).
24. S. M. Loureiro, E. V. Antipov, J. L. Tholence, J. J. Capponi, O. Chmaissem, Q. Huang, and M. Marezio, *Physica C* **217,** 253 (1993).
25. O. Chmaissem, Q. Huang, E. V. Antipov, S. N. Putilin, M. Marezio, S. M. Loureiro, J. J. Capponi, J. L. Tholence, and A. Santoro, *Physica C* **217,** 265 (1993).
26. P. Dali, B. C. Chakoumakos, G. F. Sun, K. W. Wong, Y. Xin, and D. F. Lu, *Physica C* **243,** 201 (1995).
27. J. L. Wagner, B. A. Hunter, D. G. Hinks, and J. D. Jorgensen, *Phys. Rev. B* **51,** 15407 (1995).
28. Q. Huang, O. Chmaissem, J. J. Capponi, C. Chaillout, M. Marezio, J. L. Tholence, and A. Santoro, *Physica C* **227,** 1 (1994).
29. H. M. Rietveld, *J. Appl. Crystallogr.* **2,** 65 (1969).
30. A. C. Larson and R. B. Von Dreele, ''GSAS—General Structure Analysis System,'' Rept. LA-UR-86-748, Los Alamos National Laboratory, Los Alamos, NM 87545, (1990).
31. P. Thompson, D. E. Cox, and J. B. Hastings, *J. Appl. Crystallogr.* **20,** 79 (1987).
32. R. B. Von Dreele, ''Modern Powder Diffraction'' (D. L. Bish and J. E. Post, Eds.), p. 333. The Mineralogical Society of America, Washington, 1989.
33. G. Caglioti, A. Paoletti, and F. P. Ricci, *Nucl. Instrum.* **3,** 223 (1958).
34. V. F. Sears, ''Methods of Experimental Physics, Vol 23, Part A'' (K. Skold and D. L. Price, Eds.), p. 521. Academic Press, Orlando, 1986.
35. C. C. Toradi, ''Chemistry of Superconducting Materials'' (T. A. Vanderah, Ed.), p. 510. Noyes Publications, Park Ridge, NJ, 1992.
36. B. C. Chakoumakos and M. Paranthaman, *Physica C* **227,** 143 (1994).
37. S. N. Putilin, M. G. Rozova, D. A. Kashporov, E. V. Antipov, and L. M. Kovba, *Russ. J. Inorg. Chem.* **36,** 928 (1991).
38. Von Rudolf Hoppe, and Hans-Joachim Rohrborn, *Z. Anorg. Allg. Chem.* **329,** 110 (1964).
39. K. Aurivillius, and Inga-Britt Carlsson, *Acta Chem. Scand.* **12,** 1297 (1958).
40. K. Aurivillius, *Acta. Chem. Scand.* **18,** 1305 (1964).
41. H. Ihara, K. Tokiwa, A. Iyo, M. Hirabayashi, N. Terada, M. Tokumoto, and Y. S. Song, *Physica C* **235–240,** 981 (1994) and references therein.
42. U. Welp, G. W. Crabtree, J. L. Wagner and D. G. Hinks, *Physica C* **218,** 373 (1993).